SYSTEM OPTIMIZATION OF THERMAL MANAGEMENT PERFORMANCE OF FUEL CELL SYSTEM FOR AUTOMOBILE

by

Wenfeng BAI [*] ***and Caofeng HE***

School of Intelligent Manufacturing, Huanghuai University, Zhumadian, Henan, China

Original scientific paper
https://doi.org/10.2298/TSCI2104923B

Vehicle fuel cell systems release a large amount of heat while generating electricity. The suitable thermal management system must be built to ensure system performance and reliability. Based on the analysis of the working principle of the vehicle fuel cell thermal management system, the paper establishes a control-oriented fuel cell thermal management. The stack, air cooler, hydrogen heat exchanger, bypass valve, heat sink, and cooling water circulating pump model are taking into account. System model, and the relationship between stack current, coolant flow rate, fin surface wind speed, bypass valve opening, and fuel cell temperature are in established in simulation experiments. The paper discusses their effects on system as a whole, air coolers, hydrogen heat exchangers, and the influence of the temperature difference between the inlet and outlet of the radiator. The simulation results can provide guidance and help to design the fuel cell thermal management control system.

Key words: *fuel cell, modelling, stack temperature, temperature characteristics*

Introduction

Many automobiles have caused environmental pollution, global warming, and oil shortages, thereby prompting people to find safe and efficient energy sources. As an efficient and clean energy conversion device, fuel cells have received widespread attention in the automotive industry. The proton exchange membrane fuel cell (PEMFC) has the advantages of low operating temperature, fast start-up speed, high power generation efficiency, and mature technology. It is the most suitable as a power source for automobiles. The temperature has an essential impact on the performance and reliability of the fuel cell system. The increase in the stack temperature will increase the electrochemical reaction activity and the membrane's conductivity, which will help improve the battery's performance. However, the temperature resistance of the electrolyte membrane of PEMFC is limited, and considering the water content of the membrane, the working temperature cannot be higher than 100 °C. Besides, if the fuel cell's operating temperature is too high, the platinum particle transport will be accelerated, and the catalyst will be degraded faster, resulting in a reduction in the effective area of the catalytic layer.

There has been some literature on the temperature modelling and characteristics of fuel cells. In terms of stack temperature modelling, some scholars have proposed to reduce the dimensionality, calculation time, and memory required to reduce the complex calculation of the internal mass transfer phenomenon of the fuel cell based on maintaining the geometric resolution and the essential characteristics of the fuel cell 2-3 quantity levels. Some scholars

[*] Corresponding author, e-mail: baiwenfeng@huanghuai.edu.cn

cascade the equivalent circuits of multiple single cells to obtain the battery stack temperature model, introduce non-linear resistance to make it suitable for the entire operating temperature range, and its parameters are obtained by experimental curve fitting. In the fuel cell temperature system model, some scholars have proposed a control-oriented fuel cell intensive parameter model for predicting the temperature of the stack, the exhaust reaction gas, and the coolant outlet. Some scholars have established an 8-order non-linear fuel cell temperature system model for vehicles, verified the model with 120 kW fuel cell data, and proposed a useful reduced-order linear model [1]. Some scholars' temperature system model does not consider the increase in air temperature when the compressor compresses air and decreases hydrogen temperature when the high pressure hydrogen storage tank discharges hydrogen. Some scholars consider these two parts, but they only study the suitability of the reduced-order linear model. Based on this, this article first establishes a vehicle fuel cell thermal management model, uses the built model to study the relationship between stack current, coolant flow rate, fin surface wind speed, bypass valve opening, and fuel cell temperature, and discusses their effects on air coolers. The influence of the temperature difference between the population and the outlet of the hydrogen heat exchanger, stack and radiator provides guidance for the design of the best temperature controller for the system.

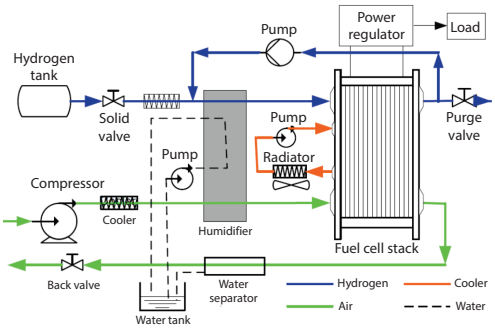

Figure 1. Fuel cell system for vehicles

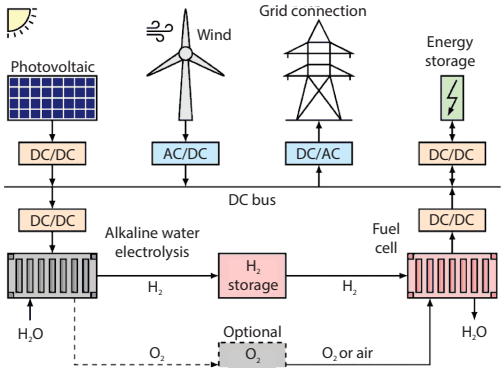

Figure 2. Energy balance of the stack system

How the thermal management system works

The fuel cell system for vehicles is shown in fig. 1. The system comprises three subsystems: the hydrogen supply system, the air supply system, and the thermal management system. The thermal management system consists of a coolant circulation pump, an air cooler, a hydrogen heat exchanger, an electric stack, a bypass valve and a heat sink, and corresponding pipe-lines [2].

Thermal management system modelling

To establish a control-oriented fuel cell thermal management system model, the paper does not consider the coolant space position's flow change and uses a lumped parameter model. We based our modelling on the following assumptions,

– the internal temperature field of each component is uniformly distributed,
– the influence of the kinetic energy and potential energy changes of the gas-flow on the system is ignored,
– the fluid temperature out of each component is assumed to be the same, and
– the constant pressure heat capacity parameters of various substances are assumed to be constants. The thermal management system modelling includes the stack, air cooler, hydrogen heat exchanger, bypass valve, heat sink, and cooling water circulation pump model.

Stack model

When a vehicle fuel cell is working, the battery's electrochemical reaction produces electricity and generates a large amount of heat, which causes the temperature of the stack to rise. The reactant gas's temperature and coolant in the stack rises and flows out of the stack through heat transfer. The gas and coolant take away a lot of heat. The signal flow diagram of the stack temperature model is shown in fig. 2. The increase in system energy is the increase in the stack's thermal energy, represented by the change in stack temperature [3].

Ignoring the heat exchange between the surface of the stack and the outside world, the thermal power obtained by the stack can be obtained from the First law of thermodynamics:

$$q_{\mathrm{st}} = P_{\mathrm{hot}} + (q_{\mathrm{ca,in}} - q_{\mathrm{ca,out}}) + (q_{\mathrm{an,in}} - q_{\mathrm{an,out}}) + (q_{\mathrm{cool,in}} - q_{\mathrm{cool,out}}) \tag{1}$$

where P_{hot} is the heating power generated by the stack and $q_{\mathrm{ca,in}}$, $q_{\mathrm{ca,out}}$ – the heating power brought and taken out of the stack cathode by the humid air, and $q_{\mathrm{an,in}}$, $q_{\mathrm{an,out}}$ – the heating power brought and taken out of the stack by the anode hydrogen. The primary material of the bipolar plate in the stack is graphite, and the heat capacity parameters can be graphite parameters:

$$q_{st} = (m_{\mathrm{st}} Cp_{\mathrm{st}} + \rho_{\mathrm{wair}} V_{\mathrm{ca}} Cp_{\mathrm{wair}} + \rho_{w\mathrm{H}_2} V_{\mathrm{an}} Cp_{\mathrm{wH}_2} + \rho_{\mathrm{cool}} V_{\mathrm{cool}} Cp_{\mathrm{cool}}) \frac{\mathrm{d}T_{\mathrm{st,c}}}{\mathrm{d}t} \tag{2}$$

where m_{st} is the mass of the stack, Cp_{st} – the heat capacity parameter of the bipolar plate, ρ_{cool} and V_{cool} – the density and volume of the coolant, respectively, ρ_{wair} and ρ_{wH_2} – the density of the cathode wet air and anode wet hydrogen, respectively, V_{ca} and V_{an} – the volume of cathode flow field and anode flow field, respectively, Cp_{wair} and Cp_{wH_2}, – the constant pressure heat capacity of cathode wet air and anode wet hydrogen, respectively, and $T_{\mathrm{st,c}}$ – the stack temperature.

Air cooler

The compressed air is sent to the cathode flow field of the fuel cell. Compressed air will cause the air temperature to rise sharply, far exceeding the set temperature range, and a cooler is required to adjust the temperature, as shown in fig. 3.

Assuming that the flow rate $m_{\mathrm{cool,inc,in}}$ of the coolant entering the air cooler is equal to the flow rate $m_{\mathrm{cool,inc,out}}$ out of it, the First law of thermodynamics:

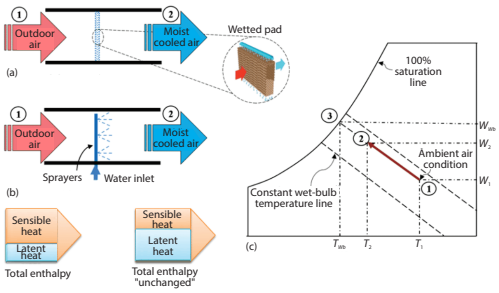

Figure 3. Air cooler; (a) wetted pad DEC, (b) sprays DEC, and (c) psychrometric chart of direct evaporative cooling process

$$\rho_{\mathrm{cool}} V_{\mathrm{inc}} Cp_{\mathrm{cool}} \frac{\mathrm{d}T_{\mathrm{inc}}}{\mathrm{d}t} = m_{\mathrm{cool,inc,out}} Cp_{\mathrm{cool}} (T_{\mathrm{inc}} - T_{\mathrm{cool,inc,in}}) + q_{\mathrm{air}} \tag{3}$$

where V_{inc} and T_{inc} are the volume and temperature of the air cooler, respectively, $T_{\mathrm{cool,inc,in}}$ – the temperature of the inflowing coolant, q_{air} – the heat power exchanged between the coolant and the air. If the flow rate $m_{\mathrm{air,inc,in}}$ of compressed air entering the air cooler is equal to the flow rate $m_{\mathrm{air,inc,out}}$ out, the thermal power q_{air} is:

$$q_{\mathrm{air}} = \varepsilon_1 m_{\mathrm{air,inc,in}} Cp_{\mathrm{air}} (T_{\mathrm{inc}} - T_{\mathrm{com}}) \tag{4}$$

where ε_1 represents the heat exchange efficiency between air and coolant, and the range is (0, 1), which can be tested according to actual conditions or can be obtained from the data provided by the equipment manufacturer [4].

Hydrogen heat exchanger

After the pressure is reduced from the high pressure hydrogen tank, the hydrogen enters the stack's anode flow field. After the pressure is reduced, the hydrogen temperature will be lower than the temperature range required by the stack, so a heat exchanger is needed to heat it. The signal diagram of the hydrogen heat exchanger is shown in fig. 4. Same as the air cooler, assuming that the flow rate $m_{\text{cool,ex,in}}$ of the coolant entering the hydrogen heat exchanger is equal to the flow rate $m_{\text{cool,ex,iout}}$ out of it:

$$\rho_{\text{cool}} V_{\text{ex}} Cp_{\text{cool}} \frac{\mathrm{d}T_{\text{ex}}}{\mathrm{d}t} = m_{\text{cool,ex,out}} Cp_{\text{cool}} (T_{\text{ex}} - T_{\text{cool,ex,in}}) + q_{\text{H}_2} \tag{5}$$

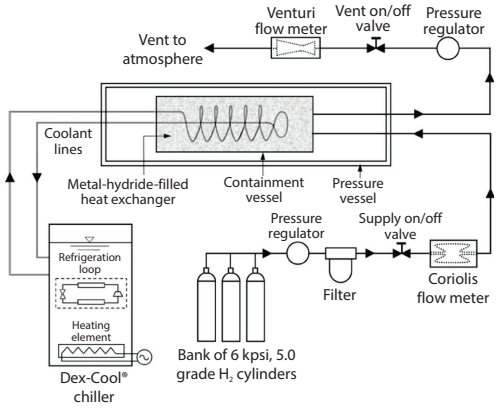

Figure 4. Hydrogen heat exchanger

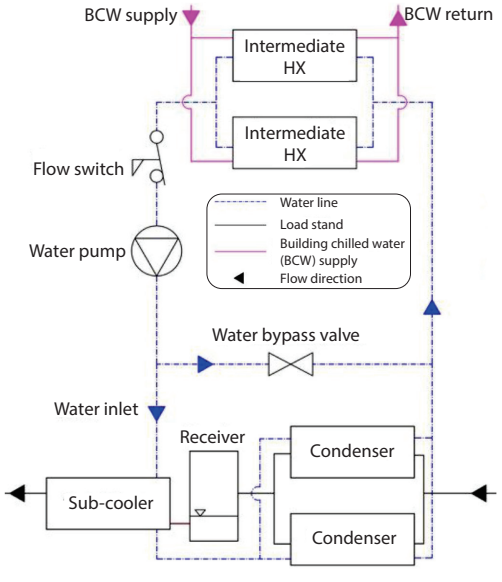

Figure 5. Bypass valve

where V_{ex} and T_{ex} are the volume and temperature of the hydrogen heat exchanger, respectively, $T_{\text{cool,ex,in}}$ – the temperature of the coolant flowing into the air cooler, and q_{H2} – the heat power exchanged between the coolant and hydrogen.

If the hydrogen flow rate $m_{\text{H2,ex,in}}$ entering the hydrogen heat exchanger is equal to the outflow flow rate $m_{\text{H2,ex,out}}$, the heating power q_{H2} can be expressed:

$$q_{\text{H}_2} = \varepsilon_2 m_{\text{H}_2} Cp_{\text{H}_2} \left(T_{\text{ex}} - T_{\text{H}_2,\text{in}}\right) \tag{6}$$

where ε_2 is the heat exchange efficiency between hydrogen and coolant, and the range is (0, 1).

Bypass valve

The bypass valve is used to adjust the flow of the coolant in the radiator. It divides the coolant into two paths: one enters the radiator, and the other enters the branch. The signal diagram is shown in fig. 5. Regarding the coolant flow through the heat sink and branch as a linear function of the valve opening:

$$\begin{aligned} m_{\text{cool,ra,in}} &= k m_{\text{cool,bv}} \\ m_{\text{cool,bp}} &= (1-k) m_{\text{cool,bv}} \end{aligned} \tag{7}$$

where $m_{\text{cool,ra,in}}$, $m_{\text{cool,bp}}$, and $m_{\text{cool,bv}}$ are the heat sink, branch, and bypass valve flow, respectively, and k is the valve opening. The value range is $0 \le k \le 1$.

Heat sink

The heat sink dissipates a large amount of waste heat generated by the stack to the surrounding environment. The model includes the heat exchange between it and the surrounding environment, which is affected by the ambient temperature, the surrounding air velocity, the coolant flow rate, and the inlet temperature. The relationship between the data can be obtained through experiments and then made into a table

for interpolation calculation. The other part is the heat exchange between it and the coolant [5]. The heat sink signal diagram is shown in fig. 6. If the incoming coolant flow rate $m_{\text{cool,ra,in}}$, is equal to the outgoing flow rate $m_{\text{cool,ra,out}}$:

$$\rho_{\text{cool}} V_{\text{ra}} Cp_{\text{cool}} \frac{\mathrm{d}T_{\text{ra}}}{\mathrm{d}t} m_{\text{cool,ra,out}} (T_{\text{ra,out}} - T_{\text{ra,in}}) - q_{\text{cir}} \quad (8)$$

where V_{ra} and T_{ra} are the volume and temperature of the heat sink, respectively, $T_{\text{ra,out}}$ – the temperature of the coolant flowing into the heat sink, and q_{cir} – the heat power transferred from the heat sink to the surrounding environment.

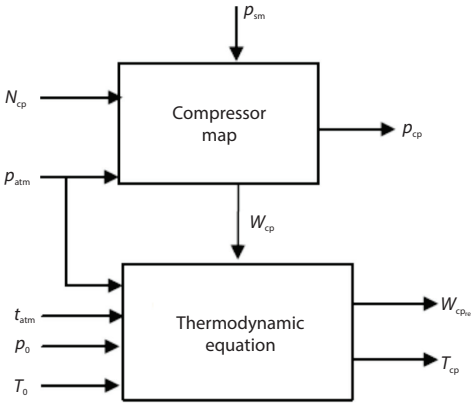

Figure 6. Heat sink

Coolant circulation pump

The coolant circulation pump provides power for the coolant to flow between the components and the pipe-line. Under its rated working speed, its output flow:

$$Q_{we} = a_3 p_w^3 + a_2 p_w^2 + a_1 p_w + a_0 \quad (9)$$

In actual work, the rotation speed of the circulating pump is often not at the rated speed. Using a similar principle, the output flow Q_{wN} at this time:

$$Q_{wN} = \left(\frac{N}{N_e} \right) Q_{we} \quad (10)$$

Considering the speed's dynamic response time, the first-order inertia link can be used, namely $1/(1 + T_p s)$, where T_p is the time constant.

Simulation results and analysis

This article models the thermal management system of BALLARD's Mark 902 (85 kW) fuel cell. The data used comes from the experimental data in published literature and BALLARD's product specification. In the simulation, the air excess coefficient is 1.8, the hydrogen excess coefficient is 1.6, the pressure of the cooling water flow field is $1.22 \cdot 10^4$ Pa lower than the cathode flow field's pressure, and the temperature of the supplied coolant is 50 °C.

Analysis of steady-state characteristics

The relationship between stack current and its temperature

When the bypass valve coefficient is 1, the circulating pump speed is 2000 rpm, and the stack current is, respectively 200 A and 300 A, the wind speed on the radiator surface varies from 1 to 8 m/s. The simulation results are shown in fig. 7. It can be seen from the figure that under the condition of constant stack current, as the wind speed on the surface of the ra-

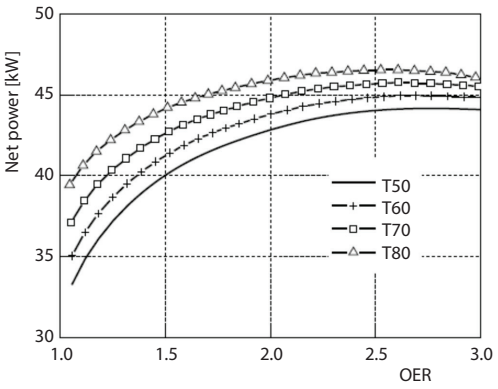

Figure 7. Stack current and temperature characteristics

diator increases, the stack inlet and outlet temperatures gradually decrease. Under the same heat dissipation conditions, the greater the stack current, the higher the stack population and outlet temperature [6]. When the wind speed is 6-8 m/s, the stack temperature does not change with the wind speed increase. The reason is that the temperature of the supplied coolant is set to 50 °C. According to the simulation results, the wind speed must be greater than 4.2 m/s when the current is 200 A, and the wind speed must be greater than 5.3 m/s when the current is 300 A to ensure that the coolant inlet temperature is within the expected range (the stack inlet coolant temperature is expected to be 50-65 °C). It can be seen that the greater the current, the greater the heat power generated by the battery reaction, and a higher wind speed is required to dissipate this heat.

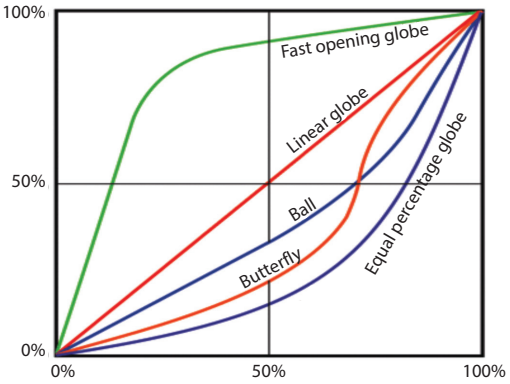

Figure 8. Valve opening and temperature characteristics

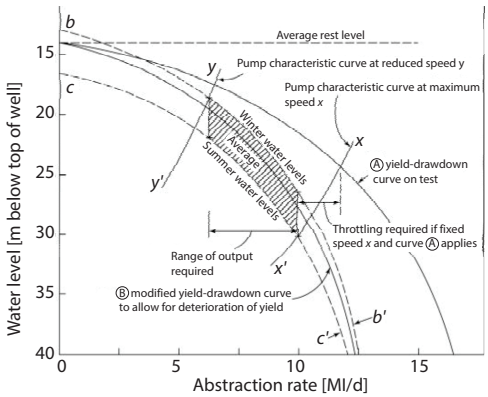

Figure 9. Circulating pump speed and temperature characteristics

The influence of bypass valve coefficient on stack temperature

The circulating pump speed is 2000 rpm, the bypass valve coefficient varies from 0.1-1, the stack current is 20 A, and the wind speed is 5 m/s. The simulation results are shown in fig. 8. The stack temperature can be adjusted by changing the bypass valve opening, but when the valve opening is more significant than 0.5, it will hardly affect the stack temperature. The reason is that at a certain wind speed when the coolant flow in the radiator reaches an absolute value, it is affected by The heat dissipation capacity is limited, and the flow rate continues to increase while the heat dissipation power is almost unchanged [7].

The influence of circulating pump speed on stack temperature

The circulating pump's speed is 1000~2000 rpm, the valve coefficient is 0.5, the stack current is 200 A, and the wind speed is 5 m/s. The simulation results are shown in fig. 9. By adjusting the circulating pump's speed, the stack's inlet and outlet temperatures can be adjusted. When the speed reaches a particular value, the speed will continue to increase, and the stack temperature will almost remain unchanged. Simultaneously, as the rotation speed increases, the temperature difference between the exit and the stack entrance can be reduced [8].

In the case of ignoring the air and hydrogen flow fields in the stack, according to the law of thermodynamics, when the stack temperature is stable, the heating power taken by the coolant is equal to the heating power generated by the stack:

$$m_{\text{cool,st}} Cp_{\text{cool}} (T_{\text{cool,st,in}} - T_{\text{cool,st,out}}) = p_{\text{hot}} \tag{11}$$

Usually, the temperature difference between the reactor population and the outlet temperature is less than 10 °C. The flow rate of the coolant flowing through the reactor should meet:

$$m_{\text{cool,st}} \geq \frac{p_{\text{hot}}}{10 Cp_{\text{cool}}} \tag{12}$$

When the stack current is 200 A, and the temperature is 65 °C, the stack's thermal power is 69.19 kW. The calculation from eq. (12) shows that the stack's coolant flow rate should be greater than 99 standard Lpm. It can be seen in fig. 3 that when the speed is 1000 rpm (flow rate 108.64 standard Lpm), the stack temperature difference is about 10 °C, and the calculated results are consistent with the experimental results [9].

Analysis of dynamic characteristics

The stack current, the radiator's surface wind speed, and the circulating pump speed take a series of jump values, as shown in fig. 10. The bypass valve opening is unchanged at 50 °C, and the simulation results are shown in fig. 10. The temperature difference between the air cooler's outlet and inlet and the hydrogen heat exchanger is less than 1°C. Compared with the hydrogen heater, the air cooler has a massive temperature difference. The reason is that the heat generated by compressing air from atmospheric pressure to $1.8 \cdot 10^5$ Pa is greater than that of hydrogen. Reduce the heat absorbed from $3 \cdot 10^5$ Pa to $2 \cdot 10^5$ Pa. The stack current, the radiator's wind speed, and the circulating pump's rotation speed have little effect on the temperature difference at the hydrogen heat exchanger outlet. When the circulating pump speed is 1000-1600 rpm, the coolant flow rate is 1.8107-2.8971 kg/s. If the temperature difference of the hydrogen heat exchanger is 0.5 °C, the heat power brought by the coolant is 1.8573-2.8652 kW. When the stack current is 300 A, the hydrogen supplied (excess factor 1.6) is 0.2217 g/s, the temperature of the hydrogen when entering the heater is –60.75 °C, if the temperature of the hydrogen after heating is 65 °C, the heating power required for the hydrogen is 0.115 kW is much smaller than the heating power brought in by the coolant, so the temperature difference of the hydrogen heat exchanger is almost not affected by the stack current, the wind speed of the radiator and the rotation speed of the circulating pump. We consider that in the existing system, gas cylinders, pipes, valves, *etc.* will absorb heat from the environment during the hydrogen decompression process, and the hydrogen temperature cannot be so low, and the actual heat exchange is required is less [10]. Considering the complexity of the system, the existing system, the hydrogen heat exchanger can be eliminated. In the air supply system, the air compressor is often equipped with an independent thermal management system to dissipate heat from the compressor pump head, making the system more complicated. It is a feasible way to simplify the system through the fuel cell coolant entering the pump head to cool the compressed air and the pump head.

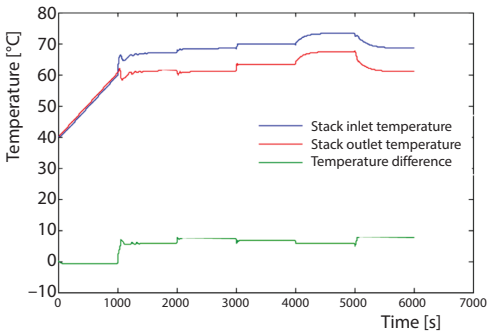

Figure 10. Stack temperature and temperature difference

At t = 1000-2600 seconds, the circulating pump speed increases, and the temperature difference of the air cooler decreases. At t = 1600 seconds, the pump speed decreases, and the

temperature difference of the heat exchanger increases. It can be seen that increasing the pump speed can reduce the temperature difference of the heat exchanger while changing the wind speed on the surface of the radiator hardly affects the temperature difference [11].

The pump speed change has almost no effect on the stack population and outlet temperature but has a slight effect on the temperature of the heat sink outlet. In the steady-state, when the pump speed is high (600 s < t < 1000 s, the 2600 s < t < 3000 s), the temperature difference between the stack population, outlet, and the heat sink outlet is small. When the pump speed is low (1600 s < t < 2000 s), the temperature difference is large. It can be seen that adjusting the coolant flow rate can improve the temperature difference between the stack and the heat sink. If the stack current is constant and the wind speed is increased, the stack's temperature will be lower due to the increase in heat dissipation. On the contrary, if the wind speed is reduced, the stack's temperature will increase. The stack's temperature is determined by the stack current and the wind speed on the surface of the heat sink.

Conclusion

In this paper, the vehicle fuel cell thermal management system is modeled, and the steady-state and dynamic characteristics are simulated. The results show that the stack temperature is affected by its current, wind speed on the radiator's surface, coolant flow rate, and the opening of the bypass valve. By controlling the speed of the radiator fan to change the wind speed on the surface of the radiator, the fuel cell coolant can be controlled within the desired temperature range, and effective thermal management of the battery system can be realized. Changing the bypass valve opening and the circulating pump speed can be to a certain extent adjust the temperature difference between the inlet and outlet of the stack. The simulation results also show that the thermal load caused by air compression and hydrogen decompression accounts for a small proportion of the fuel cell coolant system. If you consider reducing the system complexity and control accuracy, you can rely on natural heat absorption for the hydrogen circuit. The hydrogen heat exchanger is not used for hydrogen preheating for the air circuit, the coolant system can be directly used to cool the air compressor's pump head instead of a separate circulating cooling system.

Acknowledgment

This work was supported by the Science and technology research plan projects of Henan province: Research and development of new intelligent rescue robot system in mining area (No. 182102311069).

References

[1] Zhang, Q., Performance Prediction of Proton Exchange Membrane Fuel Cell Engine Thermal Management System Using 1-D and 3-D Integrating Numerical Simulation, *International Journal of Hydrogen Energy*, *43* (2018), 3, pp. 1736-1748
[2] Fletcher, T., *et al*., An Energy Management Strategy to Concurrently Optimise Fuel Consumption & PEM Fuel Cell Lifetime in a Hybrid Vehicle, *International Journal of Hydrogen Energy, 41* (2016), 46, pp. 21503-21515
[3] Wu, S., Construction of Visual 3-D Fabric Reinforced Composite Thermal Perfomance Prediction System, *Thermal Science*, *23* (2019), 5, pp. 2857-2865
[4] Yan, W. M., *et al*., Performance Improvement of Air-Breathing Proton Exchange Membrane Fuel Cell Stacks by Thermal Management, *International Journal of Hydrogen Energy*, *45* (2020), 42, pp. 22324-22339
[5] Non-obe, Y., Development of the Fuel Cell Vehicle Mirai, *IEEJ Transactions on Electrical and Electronic Engineering*, *12* (2017), 12, pp. 5-9

[6] Jaguemont, J., *et al*., Thermal Management of a Hybrid Electric Vehicle in Cold Weather, *IEEE Transactions on Energy Conversion*, *31* (2016), 3, pp. 1110-1120
[7] Lapeña-Rey, N., *et al*., A Fuel Cell Powered Unmanned Aerial Vehicle for Low Altitude Surveillance Missions, *International Journal of Hydrogen Energy, 42* (2017), 10, pp. 6926-6940
[8] Hoflinger, J., *et al*., The FCREEV a Fuel Cell Range Extended Electric Vehicle, *MTZ Worldwide*, *78* (2017), 5, pp. 18-23
[9] Marzougui, H., *et al*., Energy Management of Fuel Cell/Battery/Ultracapacitor in Electrical Hybrid Vehicle, *International Journal of Hydrogen Energy*, *42* (2017), 13, pp. 8857-8869
[10] Wu, S., Study and Evaluation of Clustering Algorithm for Solubility and Thermodynamic Data of Glycerol Derivatives, *Thermal Science*, *23* (2019), 5, pp. 2867-2875
[11] Tanc, B., *et al*., Energy Distribution Analyses of an Additional Traction Battery on Hydrogen Fuel Cell Hybrid Electric Vehicle, *International Journal of Hydrogen Energy*, *45* (2020), 49, pp. 26344-26356

Paper submitted: November 9, 2020
Paper revised: December 17, 2020
Paper accepted: January 18, 2021